Fabrication and characterization of back-side illuminated InGaN/GaN solar cells with periodic via-holes etching and Bragg mirror processes

Yi-An Chang,[1] Fang-Ming Chen,[2] Yu-Lin Tsai,[1] Ching-Wen Chang,[3] Kuo-Ju Chen,[1] Shan-Rong Li,[2] Tien-Chang Lu,[1] Hao-Chung Kuo,[1,*] Yen-Kuang Kuo,[4] Peichen Yu,[1] Chien-Chung Lin,[5] and Li-Wei Tu[3]

[1]*Department of Photonics and Institute of Electro-Optical Engineering, National Chiao Tung University, Hsinchu 30010, Taiwan*

[2]*Institute of Photonics, National Changhua University of Education, Changhua 50007, Taiwan*

[3]*Department of Physics and Center for Nanoscience and Nanotechnology, National Sun Yat-Sen University, Kaohsiung 80424, Taiwan*

[4]*Department of Physics, National Changhua University of Education, Changhua 50007, Taiwan*

[5]*Institute of Photonic System, College of Photonics, National Chiao-Tung University, Tainan 71150, Taiwan*

[*]*hckuo@faculty.nctu.edu.tw*

Abstract: In this study, the design and fabrication schemes of back-side illuminated InGaN/GaN solar cells with periodic via-holes etching and Bragg mirror processes are presented. Compared to typical front-side illuminated solar cells, the improvements of open-circuit voltage (V_{oc}) from 1.88 to 1.94 V and short-circuit current density (J_{sc}) from 0.84 to 1.02 mA/cm^2 are observed. Most significantly, the back-side illuminated InGaN/GaN solar cells exhibit an extremely high fill factor up to 85.5%, leading to a conversion efficiency of 1.69% from 0.66% of typical front-side illuminated solar cells under air mass 1.5 global illuminations. Moreover, the effects of bottom Bragg mirrors on the photovoltaic characteristics of back-side illuminated solar cells are studied by an advanced simulation program. The results show that the J_{sc} could further be improved with a factor of 10% from the original back-side illuminated solar cell by the structure optimization of bottom Bragg mirrors.

OCIS codes: (040.5350) Photovoltaic; (130.5990) Semiconductors; (230.1480) Bragg reflectors.

References and links

1. T. Matsuoka, H. Okamoto, M. Nakao, H. Harima, and E. Kurimoto, "Optical bandgap energy of wurtzite InN," Appl. Phys. Lett. **81**(7), 1246–1248 (2002).
2. N. G. Toledo, D. J. Friedman, R. M. Farrell, E. E. Perl, C.-T. Lin, J. E. Bowers, J. S. Speck, and U. K. Mishra, "Design of integrated III-nitride/non-III-nitride tandem photovoltaic devices," J. Appl. Phys. **111**, 054503 (2012).
3. S. P. Bremner, M. Y. Levy, and C. B. Honsberg, "Analysis of tandem solar cell efficiencies under AM1.5G spectrum using a rapid flux calculation method," Prog. Photovolt. Res. Appl. **16**(3), 225–233 (2008).
4. C. H. Ho, G. J. Lin, P. H. Fu, C. A. Lin, P. C. Yang, I.-M. Chan, K. Y. Lai, and J. H. He, "An efficient light-harvesting scheme using SiO2 nanorods for InGaN multiple quantum well solar cells," Sol. Energy Mater. Sol. Cells **103**, 194–198 (2012).
5. H. C. Lee, Y. K. Su, W. K. Chuang, J. C. Lin, K. C. Huang, Y. C. Cheng, and K. J. Chang, "Discussion on electrical characteristics of i-In0.13Ga0.87N p-i-n photovoltaics by using a single/multi-antireflection layer," Sol. Energy Mater. Sol. Cells **94**(7), 1259–1262 (2010).
6. C. C. Yang, C. H. Jang, J. K. Sheu, M. L. Lee, S. J. Tu, F. W. Huang, Y. H. Yeh, and W. C. Lai, "Characteristics of InGaN-based concentrator solar cells operating under 150X solar concentration," Opt. Express **19**(S4), A695–A700 (2011).
7. R. H. Horng, S. T. Lin, Y. L. Tsai, M. T. Chu, W. Y. Liao, M. H. Wu, R. M. Lin, and Y. C. Lu, "Improved conversion efficiency of GaN/InGaN thin-film solar cells," IEEE Electron Device Lett. **30**(7), 724–726 (2009).

#210763 - $15.00 USD Received 24 Apr 2014; revised 16 Jun 2014; accepted 21 Jun 2014; published 11 Aug 2014

8. C. L. Tsai, G. S. Liu, G. C. Fan, and Y. S. Lee, "Substrate-free large gap InGaN solar cells with bottom reflector," Solid-State Electron. **54**(5), 541–544 (2010).
9. E. Matioli, C. Neufeld, M. Iza, S. C. Cruz, A. A. Al-Heji, X. Chen, R. M. Farrell, S. Keller, S. DenBaars, U. Mishra, S. Nakamura, J. Speck, and C. Weisbuch, "High internal and external quantum efficiency InGaN/GaN solar cells," Appl. Phys. Lett. **98**(2), 021102 (2011).
10. C. H. Ho, D. H. Lien, H. C. Chang, C. A. Lin, C. F. Kang, M. K. Hsing, K. Y. Lai, and J. H. He, "Hierarchical structures consisting of SiO2 nanorods and p-GaN microdomes for efficiently harvesting solar energy for InGaN quantum well photovoltaic cells," Nanoscale **4**(23), 7346–7349 (2012).
11. P. H. Fu, G. J. Lin, C. H. Ho, C. A. Lin, C. F. Kang, Y. L. Lai, K. Y. Lai, and J. H. He, "Efficiency enhancement of InGaN multi-quantum-well solar cells via light-harvesting SiO2 nano-honeycombs," Appl. Phys. Lett. **100**(1), 013105 (2012).
12. G. J. Lin, K. Y. Lai, C. A. Lin, Y. L. Lai, and J. H. He, "Efficiency enhancement of InGaN-based multiple quantum well solar cells employing antireflective ZnO nanorod arrays," IEEE Electron Device Lett. **32**(8), 1104–1106 (2011).
13. G. J. Lin, K. Y. Lai, C. A. Lin, and J. H. He, "Solar energy harvesting scheme using syringe-like ZnO nanorod arrays for InGaN/GaN multiple quantum well solar cells," Opt. Lett. **37**(1), 61–63 (2012).
14. Y. L. Tsai, C. C. Lin, H. V. Han, C. K. Chang, H. C. Chen, K. J. Chen, W. C. Lai, J. K. Sheu, F. I. Lai, P. Yu, and H. C. Kuo, "Improving efficiency of InGaN/GaN multiple quantum well solar cells using CdS quantum dots and distributed Bragg reflectors," Sol. Energy Mater. Sol. Cells **117**, 531–536 (2013).
15. X. Zheng, R. H. Horng, D. S. Wuu, M. T. Chu, W. Y. Liao, M. H. Wu, R. M. Lin, and Y. C. Lu, "High-quality InGaN/GaN heterojunctions and their photovoltaic effects," Appl. Phys. Lett. **93**(26), 261108 (2008).
16. J. R. Lang, C. J. Neufeld, C. A. Hurni, S. C. Cruz, E. Matioli, U. K. Mishra, and J. S. Speck, "High external quantum efficiency and fill-factor InGaN/GaN heterojunction solar cells grown by NH3-based molecular beam epitaxy," Appl. Phys. Lett. **98**(13), 131115 (2011).
17. R. R. King, D. C. Law, K. M. Edmondson, C. M. Fetzer, G. S. Kinsey, H. Yoon, R. A. Sherif, and N. H. Karam, "40% efficient metamorphic GaInP/GaInAs/Ge multi-junction solar cells," Appl. Phys. Lett. **90**(18), 183516 (2007).
18. M. A. Green, K. Emery, Y. Hishikawa, W. Warta, and E. D. Dunlop, *Progress in Photovoltaics: Solar Cell Efficiency Tables (Version 39)* (Wiley, 2011).
19. Y. A. Chang, Z. Y. Li, H. C. Kuo, T. C. Lu, S. F. Yang, L. W. Lai, L. H. Lai, and S. C. Wang, "Efficiency improvement of single-junction InGaP solar cells fabricated by a novel micro-hole array surface texture process," Semicond. Sci. Technol. **24**(8), 085007 (2009).
20. C. J. Neufeld, S. C. Cruz, R. M. Farrell, M. Iza, S. Keller, S. Nakamura, S. P. DenBaars, J. S. Speck, and U. K. Mishra, "Observation of positive thermal power coefficient in InGaN/GaN quantum well solar cells," Appl. Phys. Lett. **99**(7), 071104 (2011).
21. S. Y. Bae, J. P. Shim, D. S. Lee, S. R. Jeon, and G. Namkoong, "Improved photovoltaic effects of a vertical-type InGaN/GaN multiple quantum well solar cell," Jpn. J. Appl. Phys. **50**, 092301 (2011).
22. G. J. Sheu, F. S. Hwu, J. C. Chen, J. K. Sheu, and W. C. Lai, "Effect of the electrode pattern on current spreading and driving voltage in a GaN/sapphire LED chip," J. Electrochem. Soc. **155**(10), H836–H840 (2008).
23. D. Raoufi, A. Kiasatpour, H. R. Fallah, and A. S. H. Rozatian, "Surface characterization and microstructure of ITO thin films at different annealing temperatures," Appl. Surf. Sci. **253**(23), 9085–9090 (2007).
24. D. J. Seo, J. P. Shim, S. B. Choi, T. H. Seo, E. K. Suh, and D. S. Lee, "Efficiency improvement in InGaN-based solar cells by indium tin oxide nano dots covered with ITO films," Opt. Express **20**(S6), A991–A996 (2012).
25. APSYS, Crosslight Software Inc, Vancouver, BC, Canada, 2012.
26. Y. K. Kuo, Y. A. Chang, H. W. Lin, J. Y. Chang, S. H. Yen, F. M. Chen, and Y. H. Chen, "Advantages of InGaN solar cells with p-doped and high-Al-content superlattice AlGaN barriers," IEEE Photon. Technol. Lett. **25**(1), 85–87 (2013).
27. J. Y. Chang, S. H. Yen, Y. A. Chang, B. T. Liou, and Y. K. Kuo, "Numerical investigation of high-efficiency InGaN-based multijunction solar cell," IEEE Trans. Electron. Dev. **60**(12), 4140–4145 (2013).
28. Y. A. Chang, Y. T. Kuo, J. Y. Chang, and Y. K. Kuo, "Investigation of InGaN green light-emitting diodes with chirped multiple quantum well structures," Opt. Lett. **37**(12), 2205–2207 (2012).
29. G. F. Brown, J. W. Ager III, W. Walukiewicz, and J. Wu, "Finite element simulations of compositionally graded InGaN solar cells," Sol. Energy Mater. Sol. Cells **94**(3), 478–483 (2010).
30. J. Piprek and Z. M. S. Li, "Origin of InGaN light-emitting diode efficiency improvements using chirped AlGaN multi-quantum barriers," Appl. Phys. Lett. **102**(2), 023510 (2013).
31. S. L. Chuang and C. S. Chang, "K•p method for strained wurtzite semiconductors," Phys. Rev. B **54**(4), 2491–2504 (1996).
32. S. L. Chuang and C. S. Chang, "A band-structure model of strained quantum-well wurtzite semiconductors," Semicond. Sci. Technol. **12**(3), 252–263 (1997).
33. I. Vurgaftman, J. R. Meyer, and L. R. Ram-Mohan, "Band parameters for III–V compound semiconductors and their alloys," J. Appl. Phys. **89**(11), 5815–5875 (2001).
34. J. Wu, "When group-III nitrides go infrared: New properties and perspectives," J. Appl. Phys. **106**(1), 011101 (2009).
35. I. Gorczyca, T. Suski, N. E. Christensen, and A. Svane, "Size effects in band gap bowing in nitride semiconducting alloys," Phys. Rev. B **83**(15), 153301 (2011).

#210763 - $15.00 USD Received 24 Apr 2014; revised 16 Jun 2014; accepted 21 Jun 2014; published 11 Aug 2014

36. G. Martin, A. Botchkarev, A. Rockett, and H. Morkoç, "Valence-band discontinuities of wurtzite GaN, AlN, and InN heterojunctions measured by x-ray photoemission spectroscopy," Appl. Phys. Lett. **68**(18), 2541–2543 (1996).
37. V. Fiorentini, F. Bernardini, and O. Ambacher, "Evidence for nonlinear macroscopic polarization in III–V nitride alloy heterostructures," Appl. Phys. Lett. **80**(7), 1204–1206 (2002).
38. A. Reale, G. Massari, A. Di Carlo, P. Lugli, A. Vinattieri, D. Alderighi, M. Colocci, F. Semond, N. Grandjean, and J. Massies, "Comprehensive description of the dynamical screening of the internal electric fields of AlGaN/GaN quantum wells in time-resolved photoluminescence experiments," J. Appl. Phys. **93**(1), 400–409 (2003).
39. M. Meneghini, N. Trivellin, G. Meneghesso, E. Zanoni, U. Zehnder, and B. Hahn, "A combined electro-optical method for the determination of the recombination parameters in InGaN-based light-emitting diodes," J. Appl. Phys. **106**(11), 114508 (2009).
40. J. Piprek, *Nitride Semiconductor Devices - Principles and Simulation* (Wiley, 2007.

1. Introduction

For the applications of converting solar energy into electricity, solar cells made from III-nitride semiconductors are regarded as the most fascinating candidate, which provides sufficient light absorption from their inherent direct-bandgap characteristics and a broad band of energy absorption covering from 0.65 to 3.43 eV [1]. This is a tremendously significant requisition for the realization of multi-junction solar cells with conversion efficiency greater than 50% [2,3]. In the development of InGaN/GaN solar cells, the fabrication scheme of device process almost remained firmly as front-side illuminated structure, in which the incident light impinged mainly upon the p-GaN layer and both p- and n-electrodes were located on topside [4–6]. Based on this process scheme, various methods for improving light coupling such as surface texturing [7,8], p-GaN roughening [9–11], anti-reflection coating [12,13] and mirror coating directly at the end of bottom sapphire substrate [14] had been applied and proven to be effective for efficiency enhancement. It shall be noted, however, that the electrode regions including the grids and pads for both p- and n-contacts must be eliminated to let more light impinging into the main p-n InGaN absorption region; nevertheless, the series resistance increases unwillingly as an expense due to the increased mean pathway for photocurrent being collected into electrodes. It becomes a trade-off between the active light-incident area and the electrode region on topside. In a prior research of typical front-side illuminated solar cells, high V_{oc} around 2.1 V and fill factor up to 81% in p-GaN/i-$In_{0.1}Ga_{0.9}N$/n-GaN solar cells, displaying conversion efficiency of 0.5% under standard air mass 1.5 global illumination had been demonstrated [15]. Lang *et al*. also presented high IQE greater than 90% and fill factor over 72% in InGaN/GaN heterojunction solar cells under air mass 0 illumination [16]. Hence, it is presumably regarded that obtaining high J_{sc} with simultaneously holding a fill factor up to 85% in typical front-side illuminated InGaN/GaN solar cells becomes an arduous task.

To approach the aforementioned limit, we presented in this study a noteworthy fabrication scheme of InGaN/GaN solar cell process as back-side illuminated structure, in which light impinged the sapphire surface, forward transparently then directly to the main p-n InGaN absorption region without considering any shading loss from electrodes. Both p- and n-electrodes were designed to be located at backside and enlarged as possible for die bonding process. Moreover, a spatially periodic via-holes etching process was presented in the first instance to ameliorate the photocurrent pathway so as to improve photocurrent collection capability, and Bragg mirror was designed to be placed closely behind the main absorption region for photon reflection. As can be seen in the following text, we found these processes enhance the conversion efficiency up to 1.69% from 0.66% of typical front-side illuminated solar cells. Conspicuously, the fill factor went up to 85.5%, which was highly adequate when compared to GaAs-based solar cells [17–19]. Furthermore, structure optimizations of bottom Bragg mirrors were studied numerically; depicting the conversion efficiency could be improved with enhancing J_{sc} by reflecting more photons to enlarge the optical generations. It

#210763 - $15.00 USD Received 24 Apr 2014; revised 16 Jun 2014; accepted 21 Jun 2014; published 11 Aug 2014

is our belief that these fabrication technologies are significant and shall be considered circumspectly for the design of next generation InGaN/GaN solar cells.

2. Experiments, PV characteristics and discussions

In this study, the InGaN/GaN solar cells were grown on *c*-plane sapphire substrates by low-pressure metal-organic chemical-vapor deposition (MOCVD). A 25 nm thick low temperature GaN nucleation layer was grown at 545 °C firstly, followed by a 2.5 μm thick undoped GaN and a 2 μm thick Si-doped GaN at 1050 °C. Then, the growth temperature was linearly decreased to 750 °C to grow the absorption region, which mainly comprised ten periods of undoped $In_{0.17}Ga_{0.83}N$ (3.5 nm)/GaN (6.5 nm) MQWs. The temperature was afterwards increased to 1050 °C for growing a 20 nm thick Mg-doped $Al_{0.13}Ga_{0.87}N$ layer, followed by a 150 nm thick Mg-doped GaN contact layer to complete the structure. After MOCVD growth, two fabrication processes including typical front-side illuminated design and back-side illuminated design with periodic via-holes and Bragg mirror were implemented for comparison. For typical front-side illuminated solar cells, the fabrication process began by partially etching with reactive ion etching from the surface of p-GaN contact layer until n-type GaN was exposed, followed by depositing transparent contact layer (TCL) with a thickness around 180 nm as current spreading layer, and Cr/Au alloys were deposited to form p- and n-electrodes. Meanwhile, the fabrication process of back-side illuminated solar cells began by depositing SiO_2, grown by plasma enhanced chemical vapor deposition (PECVD) as an etching mask for partially excavating some specific via-holes on the surface to n-GaN layer by inductively coupled plasma (ICP). Then, TCL was evaporated selectively onto the p-GaN layer by e-beam evaporator, followed by depositing 4-pairs TiO_2/SiO_2 distributed Bragg reflectors (DBRs) and Ti/Al/Ti/Au metals. Afterwards, a thick SiO_2 layer was evaporated and some specific regions on the surface were excavated again for subsequent deposition of n- and p-metal contacts. Thermal annealing was then performed at 450 °C to improve the electrical properties of the contacts. Finally, the sapphire substrate was lapped and slightly polished to 150 μm, and laser scribing and breaking were utilized to have 500 × 1000 μm^2 solar cell chips. These solar cells were mounted onto 2835 lead frames and soldering-reflow bonding process was utilized in back-side illuminated solar cells for photovoltaic characteristics measurements.

Schematic plots of typical front-side and back-side illuminated InGaN/GaN solar cell structures and the optical microscope pictures taken from topsides are shown respectively in Fig. 1. As depicted in Fig. 1(b), the via-holes excavated with larger aperture (40 μm in diameter) are distributed symmetrically as n-contacts and located at the centers of hexagonal regions formed by the smaller via-holes with an aperture of 10 μm in diameter as p-contacts. Compared to typical front-side illuminated design, this symmetrical distributions of p- and n-contact via-holes in back-side illuminated solar cells is to collect the photon-generated carriers in shortest pathway, and the gap between contact layers is isolated by a thick high-quality SiO_2 passivation layer to prevent leakage current.

#210763 - $15.00 USD Received 24 Apr 2014; revised 16 Jun 2014; accepted 21 Jun 2014; published 11 Aug 2014

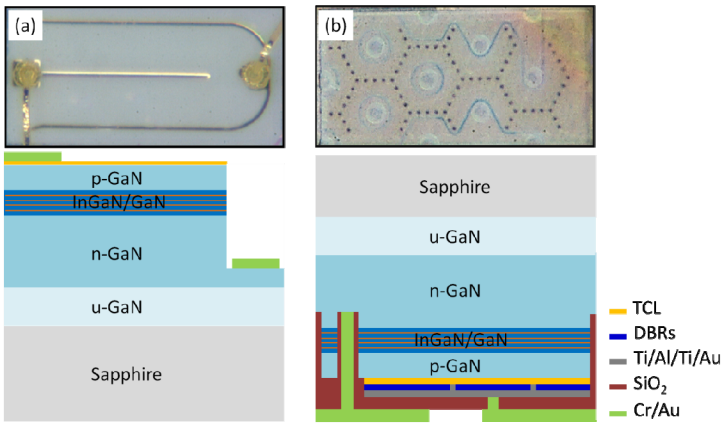

Fig. 1. Schematic plots of the fabricated InGaN/GaN solar cells with (a) typical front-side illuminated design and (b) back-side illuminated design with periodic via-holes etching and Bragg mirror processes.

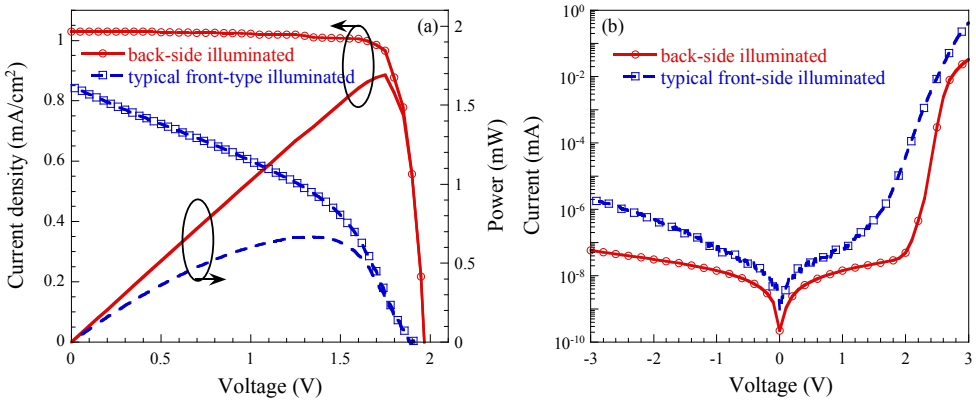

Fig. 2. J–V characteristics of typical front-side and back-side illuminated InGaN/GaN solar cells under (a) air mass 1.5 global illuminations and (b) dark situation.

Figure 2(a) shows the photovoltaic current density versus voltage (J–V) characteristics of typical front-side and back-side illuminated solar cells. A class-A solar simulator with a xenon flash tube of IEC 904–9 standard is utilized in this measurement. The incident light intensity is 100 mW/cm^2 as standard air mass 1.5 global illuminations. The spectrum of solar simulator is measured using a calibrated spectral radiometer (Soma S-2440) in a wavelength range from 300 nm to 1000 nm. The temperature is maintained at 25 °C during the measurements using an automatic temperature control system. From these measurements, the results show that the back-side illuminated solar cells with periodic via-holes etching and Bragg mirror processes can effectively enhance J_{sc} from 0.84 to 1.02 mA/cm^2, V_{oc} from 1.88 to 1.94 V, fill factor from 41.6% to 85.5% and the conversion efficiency from 0.66% to 1.69%, corresponding to a 156% enhancement compared to the typical front-side illuminated solar cells. Comparing to other research results with similar structures [20,21], the relatively lower fill factor obtained in our typical front-side illuminated solar cells may be attributed to the relatively worse metal contacts and the lack of surface and sidewall passivation that may induce larger series resistance and surface recombinations. The improvement in J_{sc} can be attributed to two main factors: one is the bottom Bragg mirror, which reflects more photons back into InGaN MQW absorption region and lengthens the optical path, promoting more

#210763 - $15.00 USD Received 24 Apr 2014; revised 16 Jun 2014; accepted 21 Jun 2014; published 11 Aug 2014

optical generations; another is the better refractive index match at interface between air (n = 1) and sapphire (n = 1.76), which acts as a window light-guiding layer, reducing top surface Fresnel reflection losses. It can also be observed in Fig. 2(b) that the dark current of back-side illuminated solar cells is approximately one order of magnitude lower than that with typical front-side illuminated solar cells when biased at −3 V, which provides the evidence of the reduction in leakage and the improvement in electrical properties. Furthermore, the ideality factors are evaluated to be 6.54 and 4.73 for typical front-side and back-side illuminated solar cells, respectively. Lower ideality factor observed in back-side illuminated solar cells may be attributed to the increase of shunt resistance and the decrease of series resistance due to better photocurrent collection capability.

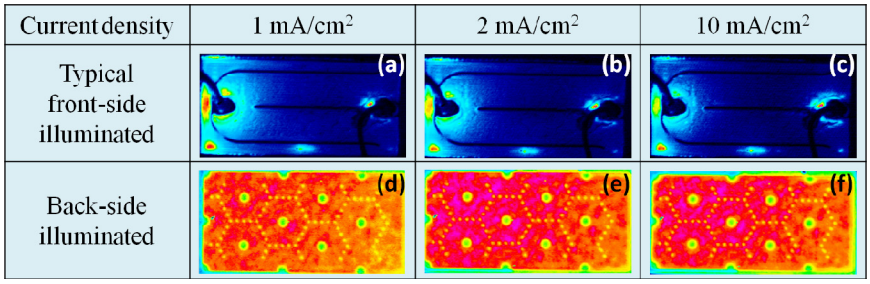

Fig. 3. Micrographs of experimentally optical emission images of (a)–(c) typical front-side and (d)–(f) back-side illuminated InGaN/GaN solar cells with different forward current densities.

As shown in Fig. 3, the analysis of near-field optical emission images observed by using a charge-coupled device camera during forward current injection are depicted to further investigate the photocurrent collection capabilities of typical front-side and back-side illuminated solar cells. The region of highest optical emission intensity is presented in red color. In general, the uniformity of luminescent pattern reflects current spreading characteristics of light-emitting devices, in which higher uniformity represents better current spreading [22]. For solar cells, the photocurrent collection capability, which can be defined as the carriers generated by photons from the absorption region flowing into electrodes without being recombined, can be regarded as a reverse mechanism of forward current injection/spreading. Therefore, luminescent patterns obtained when the solar cells are applied at forward current injection can provide a guideline of diagnosing photocurrent collection capability. As shown in Figs. 3(a)–3(c) the highest optical emission intensity always occurs near the bonding pads in typical front-side illuminated solar cells and the current distribution becomes less uniform when increasing forward currents. In contrast, the optical emission intensity shows more uniform and the luminescent patterns almost remain unchanged with increasing forward current in Figs. 3(d)–3(f). It manifests adequately that the photocurrent collection capability is apparently improved in back-side illuminated solar cells with periodic via-holes etching process. Consequently, an extremely high fill factor of 85.5% in InGaN/GaN solar cells is achieved.

3. Numerical simulation and analysis

Reflectance spectra of the Bragg mirror prepared by the progressive depositions of TCL/DBRs/metal films on a glass substrate tagging along with experimental fabrication processes, measured at normal light incident angle and the theoretical calculation are shown in Fig. 4(a). One can observe that a peak reflectance of around 86% is measured at 460 nm and can still be maintained as 72% at 400 nm of experiments, while it is visibly observed that the simulated reflectance spectrum shows good agreement near DBR stopband region. Compared to typical front-side illuminated solar cells in this study, the factor of enlarged J_{sc} due to high-reflectance bottom Bragg mirror in back-side illuminated solar cells is evident. In

#210763 - $15.00 USD Received 24 Apr 2014; revised 16 Jun 2014; accepted 21 Jun 2014; published 11 Aug 2014

addition, we'd like to underscore that the reflectance obtained in experiments can be greater if the TCL surface is smooth because the deposition of TCL film by e-beam evaporator is regarded inhomogeneous [23,24]. Two optimized Bragg mirrors, which include reducing TCL thickness to 60 nm and further modifying the thickness of DBR stacks towards a DBR stopband center in violet-blue region, and of a standard Ni (3 Å)/Ag (4000 Å) metal reflector are presented for better reflectance spectra. The phenomenon of surface roughness is neglected in our calculations; however, the position of TCL film in Bragg mirror shall be noted since the first interface for the photons being reflected at backside is p-GaN/TCL and the whole reflectance spectrum is influenced undoubtedly. As taking TCL film as one stack of DBRs, the thickness is reduced to 60 nm by defining a central wavelength of 460 nm in back-side illuminated solar cells. It is clearly seen that this optimal structure can have a wider stopband and the reflectance is improved at wavelengths above 400 nm, having a peak value of 96% at 440 nm.

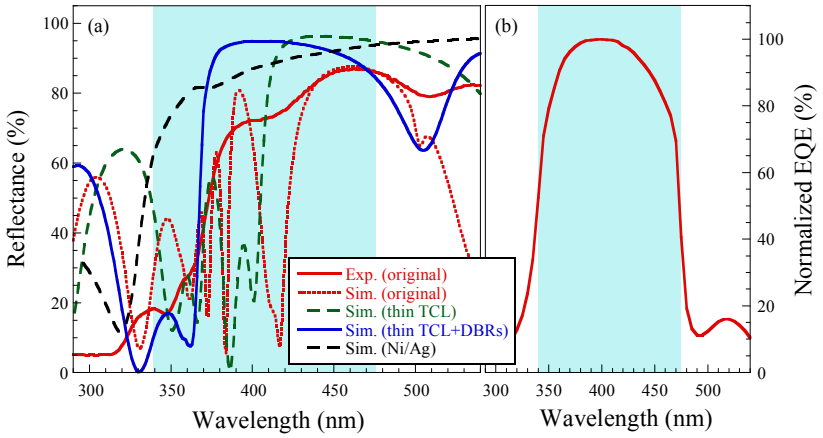

Fig. 4. (a) Reflectance spectra of the bottom Bragg mirrors and Ni/Ag metal reflector and (b) Measured EQE of back-side illuminated InGaN/GaN solar cells.

Figure 4(b) shows experimental measurement of the external QE spectrum of back-side illuminated InGaN/GaN solar cells. The results depict that the highest EQE is reached at 400 nm. The EQE spectra yield fruitful insights about the photon-to-carrier quantum efficiency in InGaN/GaN MQWs and suggest that a spectral region of 340 – 475 nm shall be covered by the reflectance spectra provided from bottom reflectors for more contributions to EQE. Therefore, relying on these aspects, another advanced Bragg mirror of shifting the stopband center toward 400 nm by reducing 24% DBR thickness while the TCL thickness remains 60 nm is presented. Compared to original Bragg mirror and the one with thin TCL in Fig. 4(a), the reflectance in ultraviolet-to-violet region is remarkably improved. The reflectance shows enhanced at wavelengths above 370 nm and reaches to 95% as tiptop at 400 nm. Besides, the reflectance spectrum of a typical Ni/Ag metal reflector is also presented for comparison. The reflectance increases gradually from 80% to 90% at wavelengths ranging from 380 to 460 nm. It can be concluded that better reflectance spectra provided by the optimized Bragg mirrors and Ni/Ag metal reflector are observed and we believe that the photovoltaic characteristics of back-side illuminated InGaN/GaN solar cells can be improved if these optimized reflectors are implemented.

Further progresses of the photovoltaic characteristics of back-side illuminated InGaN/GaN solar cells with the aforesaid optimized Bragg mirrors and Ni/Ag metal reflector are studied numerically with the APSYS advanced simulation program, which is widely used

#210763 - $15.00 USD Received 24 Apr 2014; revised 16 Jun 2014; accepted 21 Jun 2014; published 11 Aug 2014

to give an insightful review in optoelectronic devices [25–30]. The simulator employs 6 × 6 k·p model developed for the strained wurtzite semiconductor by Chuang and Chang [31,32] to calculate the energy band structures, also the interactions between photons and carriers including absorptions, generations, recombinations, and transportations are taken into calculations. The unstrained energy bandgaps for InGaN, AlGaN, and AlInN are governed by the formula proposed by Vurgaftman *et al*. [33], where the energy bandgaps of InN, GaN, and AlN are 0.641 eV, 3.424 eV, and 6.14 eV at 300 K, and the bowing parameters of InGaN, AlGaN, and AlInN are 2.0 eV, 0.24 eV, and 3.6 eV, respectively [34,35]. The band offset ratio is assumed to be 0.7/0.3 for III-nitride material systems [36]. The built-in polarization is considered at the hetero-interfaces in which the polarization induced interface charge density is calculated with the method developed by Fiorentini *et al*. [37] while the charges at hetero-interfaces are assumed to be with 20% screening. Shockley-Read-Hall (SRH) recombination lifetime and Auger recombination coefficient are set to be 10 ns and 1×10^{-30} cm^6/s, respectively [38,39]. Other material parameters used in the simulation can be found in [40].

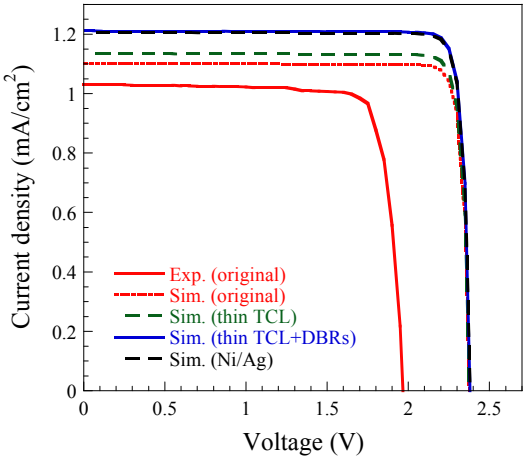

Fig. 5. Experimental and simulated J–V characteristics of back-side illuminated InGaN/GaN solar cells with original and optimized Bragg mirrors and Ni/Ag metal reflector under air mass 1.5 global illuminations.

Table 1. Device parameters of back-side illuminated InGaN/GaN solar cells with original and optimized Bragg mirrors and Ni/Ag metal reflector.

Back-side illuminated solar cells		V_{oc} (V)	J_{sc} (mA/cm^2)	Fill factor (%)	Efficiency (%)
Experiment	Original	1.94	1.02	85.5	1.69
Simulation	Original	2.38	1.10	90.6	2.37
	Thin TCL	2.38	1.14	90.1	2.44
	Thin TCL + DBRs	2.38	1.21	90.6	2.61
	Ni/Ag	2.38	1.20	90.6	2.60

Compared to experiments, the simulated J–V characteristics of the back-side illuminated solar cells with original and optimized Bragg mirrors and Ni/Ag metal reflector under air mass 1.5 global illuminations are shown in Fig. 5. Device parameters are summarized in Table 1. The comparison highlights that both two optimized Bragg mirrors and Ni/Ag metal reflector can efficiently enhance J_{sc} from original 1.1 to 1.14, 1.21 and 1.20 mA/cm^2, which corresponds to 3.6%, 10% and 9.1% enhancements respectively, compared to the original Bragg mirror in simulations.

#210763 - $15.00 USD Received 24 Apr 2014; revised 16 Jun 2014; accepted 21 Jun 2014; published 11 Aug 2014

4. Conclusion

In summary, the improved photocurrent collection and conversion efficiencies of back-side illuminated InGaN/GaN solar cells with periodic via-holes etching and Bragg mirror processes were investigated. As compared to typical front-side illuminated solar cells, an increase of 156% in conversion efficiency was achieved, and we found that it was mainly attributed to the improvements in J_{sc} and fill factor. This novel fabrication process scheme offers a more uniform and shorter pathway for photon-generated carriers to be collected into electrodes and better bottom reflectance for more optical generations. Further improvements in J_{sc} and conversion efficiencies were also investigated numerically by the optimization of bottom Bragg mirror structures. We believe that these fabrication process technologies shown in this study could give an impetus of efficiency improvement in InGaN/GaN solar cells.

Acknowledgments

This work was supported by the National Science Council, Taiwan, under Grants NSC-102-3113-P-009-007-CC2, NSC-102-2221-E-009-131-MY3 and NSC-102-2112-M-018-004-MY3.

#210763 - $15.00 USD Received 24 Apr 2014; revised 16 Jun 2014; accepted 21 Jun 2014; published 11 Aug 2014